Available online at www.sciencedirect.com
SCIENCE DIRECT®
International Journal of Heat and Mass Transfer 49 (2006) 2626–2635
International Journal of HEAT and MASS TRANSFER
www.elsevier.com/locate/ijhmt

Conduction tree networks with loops for cooling a heat generating volume

L.A.O. Rocha [a], S. Lorente [b], A. Bejan [c,*]

[a] Departamento de Física, Fundação Universidade Federal de Rio Grande, Cx. P. 474, Rio Grande, RS 96201-900, Brazil
[b] Laboratoire Matériaux et Durabilité des Constructions, Institut National des Sciences Appliquées (INSA), 135 Avenue de Rangueil, Toulouse 31077, France
[c] Department of Mechanical Engineering and Materials Science, Box 90300, Duke University, Durham, NC 27708-0300, USA

Received 31 August 2005; received in revised form 9 January 2006
Available online 10 March 2006

Abstract

Tree-shaped networks are now being considered as small-scale architectures for high-densities in electronics cooling and fuel cells design. This paper documents the optimization of tree-shaped inserts of high thermal conductivity. The new feature is the presence of loops in the tree canopy. Every feature of the tree-with-loops architecture is optimized numerically. Two classes of trees with loops are considered: loops with one size, and loops with two sizes. The performance of trees with loops is compared with that of trees without loops and designs with purely radial inserts. It is shown that dendrites and loops are features that become attractive as scales decrease and complexity increases. In the same direction, the robustness of tree-with-loops architectures increases.

Keywords: Constructal; Tree networks; Loops; Electronics cooling; Conductive inserts

1. Introduction

The progress toward smaller scales in electronics and the cooling architectures for electronics packages puts a progressively higher price on space. This means that at small enough scales convection ceases as a viable solution for cooling: the space that the fluid-filled cooling channels would occupy is just too valuable not to be allocated to electronics. In this limit, the way to channel the generated heat out of each small volume element is by installing appropriately shaped and placed inserts of high-conductivity.

Conductive inserts are architecturally analogous to the classical fins used in convection. They can be viewed as extended surfaces (needles, blades) that invade the medium, and conduct away the stream of generated heat. Just like in the design of classical fins, where compactness has led to assemblies of fins (arrays, bushes), the maximization of heat transfer density in conduction has led to tree-shaped inserts. This technological step coincided with the emergence of constructal theory [1–5], according to which flow structures such as trees are deterministic results of a principle of maximization of flow access in configurations that are free to morph. The literature on tree-shaped flow architectures is expanding rapidly, not only in electronics cooling, but also in fuel cells, heat exchangers, fluid distribution systems, augmentation, chemical reactors, product platform design, etc. [6–26].

In this paper, we examine a new class of tree-shaped structures for conduction cooling: trees with loops. This direction of inquiry is bio-inspired, because "trees with loops" is the basic architecture for leaf venation. We examine how loops and complexity affect the optimized architecture and its maximized global performance and robustness. We also compare the architecture and performance of trees with loops with older tree architectures without loops [27].

* Corresponding author. Tel.: +1 919 660 5309; fax: +1 919 660 8963.
E-mail address: dalford@duke.edu (A. Bejan).

0017-9310/$ - see front matter © 2006 Elsevier Ltd. All rights reserved.
doi:10.1016/j.ijheatmasstransfer.2006.01.017

Nomenclature

$A_{0,1}$	area, m^2
A_p	area covered by k_p material, m^2
d	the smallest length scale, m
D	thickness
i	order of tree link or construct
k_0	thermal conductivity of heat generating material, $W\,m^{-1}\,K^{-1}$
k_p	high thermal conductivity, $W\,m^{-1}\,K^{-1}$
$\tilde{k}$	conductivity ratio, k_p/k_0
L	length, m
N	number of spots on the rim touched by k_p blades
q'''	volumetric heat generation rate, $W\,m^{-3}$
R_0	disc radius, m
T	temperature, K
x	radial coordinate, m
y	transversal coordinate, m

Greek symbols

β	angle, rad
ϕ	area ratio, A_p/A

Subscripts

max	maximum
min	minimum
mm	minimized twice
mmm	minimized three times
opt	optimum
p	high-conductivity path

Superscript

(~)	dimensionless, Eq. (7)

2. One loop size, one branching level

Consider first the two-dimensional structure with loops of one size shown in Fig. 1. The structure consists of blades of high-conductivity (k_p) embedded in a heat-generating disc of radius R_0 and lower conductivity k_0. There are two blade sizes, (D_0, L_0) and (D_1, L_1), where the L's are lengths and the D's are thicknesses.

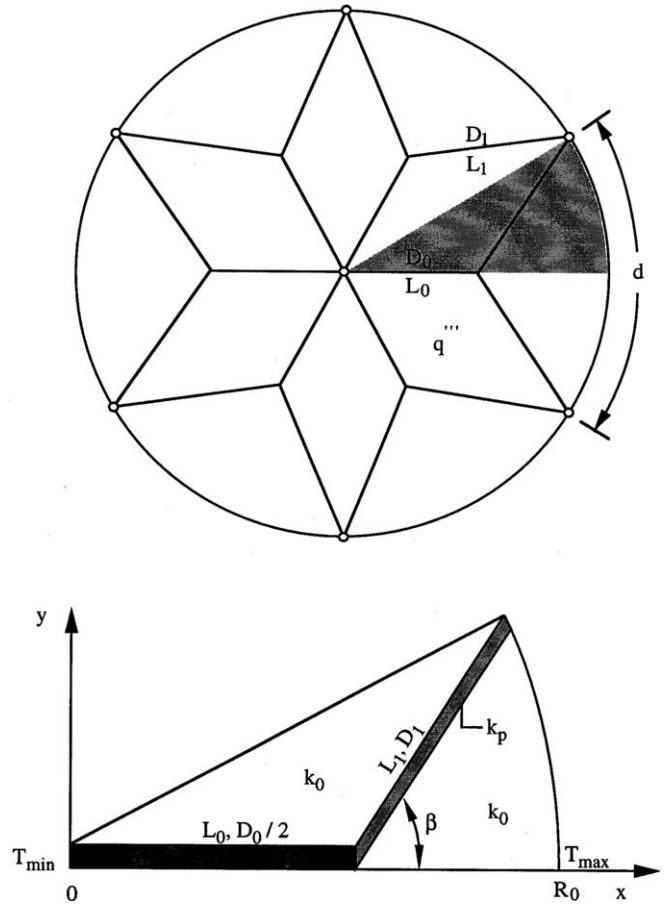

Fig. 1. Disc-shaped body with uniform heat generation, central heat sink, high-conductivity blades, loops of one size, and one level of bifurcation or pairing.

There are N points where the structure touches the rim. The structure is an assembly of trees with only one level of bifurcation, where each L_0 blade is continued by two L_1 blades. The assembly is such that each of the N points on the rim is touched by two of the branched trees. This last feature generates the loops, which are quadrilateral. In this configuration the number of blades that touch the center (n_0) is equal to N.

Heat is generated steadily in the k_0 material, and the volumetric heat generation rate is uniform, q'''. The heat current integrated over the entire disc ($q'''\pi R_0^2$) is collected by the k_p blades and channeled to the center of the disc, which serves as heat sink of temperature T_{min}. The rim is insulated. The highest temperature T_{max} occurs on the rim, in the spots where the radius that is collinear with L_0 intersects the rim. The global thermal resistance of this heat flow structure is expressed in dimensionless form by

$$\widetilde{T}_{max} = \frac{T_{max} - T_{min}}{q''' R_0^2 / k_0} \tag{1}$$

The objective is to morph the flow structure in every possible way so that its global resistance $\widetilde{T}_{max}$ is minimized. There are several constraints to consider. One is the disc radius R_0. If, in addition, we fix the distance d between two consecutive k_p-points on the rim, then the number of peripheral points is fixed ($N = 2\pi R_0/d$), and so is the area of the sector shown in the lower part of Fig. 1:

$$A_0 = \frac{\pi R_0^2}{2N} \tag{2}$$

Symmetry allows us to focus on heat conduction in the sector of area A_0. The perimeter of this area is insulated,

with the exception of the heat sink (T_{min}). An important constraint is the total amount of k_p material, which is represented by the total cross-sectional area of the blades present in A_0, namely

$$A_p = L_0 \frac{D_0}{2} + L_1 D_1 \tag{3}$$

Alternatively, the A_p and A_0 constraints can be combined to define the fixed volume fraction occupied by k_0 material,

$$\phi = \frac{A_p}{A_0} \tag{4}$$

The structure of Fig. 1 was optimized numerically by simulating the temperature field in a large number of configurations, calculating the global resistance $\widetilde{T}_{max}$, and seeking morphological changes that induce decreases in $\widetilde{T}_{max}$. The equations governing steady state conduction in the k_0 and k_p regions are, respectively

$$\frac{\partial^2 \widetilde{T}}{\partial \tilde{x}^2} + \frac{\partial^2 \widetilde{T}}{\partial \tilde{y}^2} + 1 = 0 \tag{5}$$

$$\frac{\partial^2 \widetilde{T}}{\partial \tilde{x}^2} + \frac{\partial^2 \widetilde{T}}{\partial \tilde{y}^2} = 0 \tag{6}$$

The dimensionless variables are defined as

$$(\tilde{x}, \tilde{y}, \widetilde{D}, \widetilde{L}) = \frac{(x, y, D, L)}{R_0} \qquad \widetilde{T} = \frac{T - T_{min}}{q''' R_0^2 / k_0} \tag{7}$$

Eqs. (5) and (6) were solved by using a finite elements code [28] based on triangular elements. The grid was non-uniform in both $\tilde{x}$- and $\tilde{y}$-directions, and varied from one geometry to the next. The appropriate mesh size was determined by successive refinements, quadrupling the number of elements from one mesh size to the next mesh size until the criterion $|(\widetilde{T}^j_{max} - \widetilde{T}^{j+1}_{max})/\widetilde{T}^j_{max}| < 5 \times 10^{-4}$ is satisfied. Here $\widetilde{T}^j_{max}$ represents the maximum temperature calculated using the current mesh, and $\widetilde{T}^{j+1}_{max}$ corresponds to the next mesh, where the number of elements was quadrupled. Table 1 shows an example of how grid independence was achieved. The following results were obtained by using between 4000 and 40,000 triangular elements.

The accuracy of these numerical results were tested by solving Eqs. (5) and (6) using our own MATLAB partial

Table 1
Numerical tests showing the achievement of grid independence ($N = 6$, $D_1/D_0 = 0.5$, $k_p/k_0 = 100$, $L_0 = 0.72$, $\phi = 0.1$)

Number of elements	$\widetilde{T}_{max}$	$\lvert(\widetilde{T}^j_{max} - \widetilde{T}^{j+1}_{max})/\widetilde{T}^j_{max}\rvert$
1201	0.107953	9.634×10^{-4}
4804	0.108057	4.442×10^{-4}
19,216	0.108105	1.942×10^{-4}
76,864	0.108126	

Table 2
Comparison between analytical [27] and numerical results ($\phi = 0.1$ and $\tilde{k} = 300$)

$\widetilde{R}$	$(\widetilde{L}_0)_{opt}$	$(D_0/D_1)_{opt}$	N	$(\widetilde{T}_{max})_{min}$ [27]	$(\widetilde{T}_{max})_{min}$
2.3	0.1237	2.112	7.860	0.1894	0.2197
2.5	0.3269	2.139	8.533	0.2094	0.2344
3.0	0.8341	2.162	10.21	0.2712	0.2742
3.5	1.3515	2.290	11.81	0.3425	0.3204
4.0	1.8664	2.367	13.41	0.4225	0.3745
6.0	3.9224	2.636	19.58	0.8356	0.6855
8.0	5.9645	2.833	25.58	1.4030	1.1611
10.0	7.9945	2.978	31.50	2.1317	1.8085

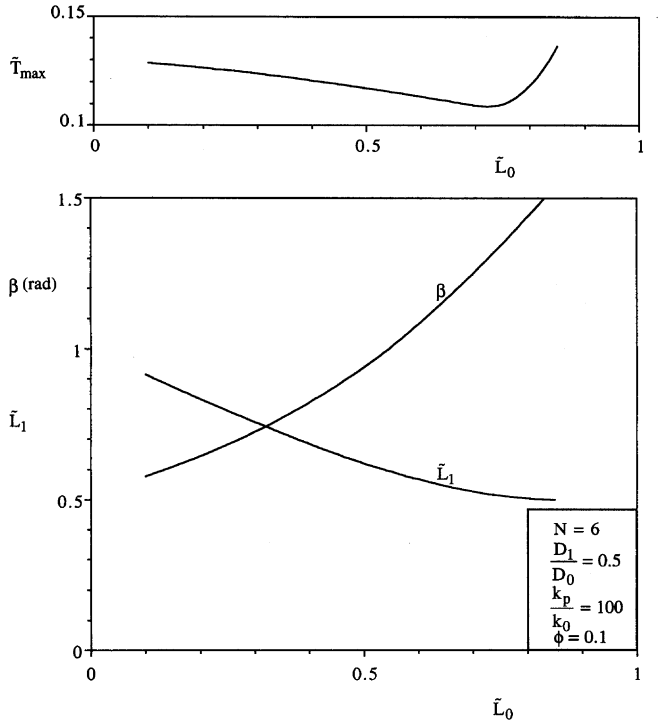

Fig. 2. The minimization of the overall thermal resistance with respect to the central blade length $\widetilde{L}_0$.

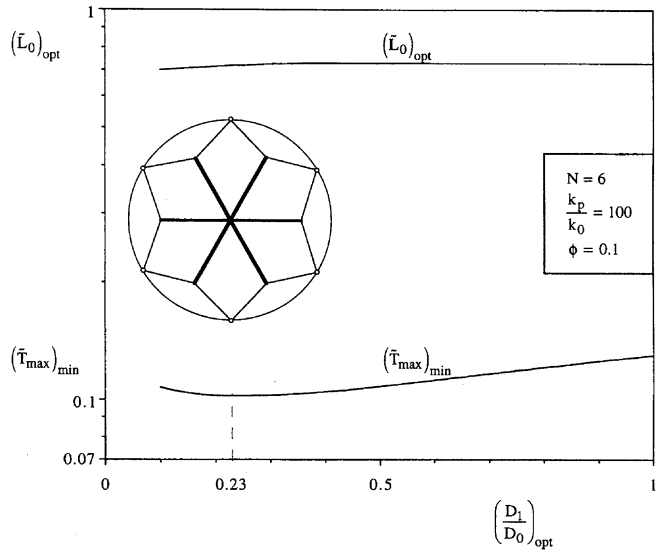

Fig. 3. The minimization with respect to D_1/D_0 of the global resistance already minimized with respect to $\widetilde{L}_0$.

differential equations toolbox code [28] and comparing the results with the analytical results reported in Rocha et al. [27] for the domain shown in Fig. 8 (see Section 3). Table 2 shows that the numerical and analytical results agree within 18%. They agree even better (within 1%) when $N \cong 10$, because the assumptions used in Ref. [27] are more

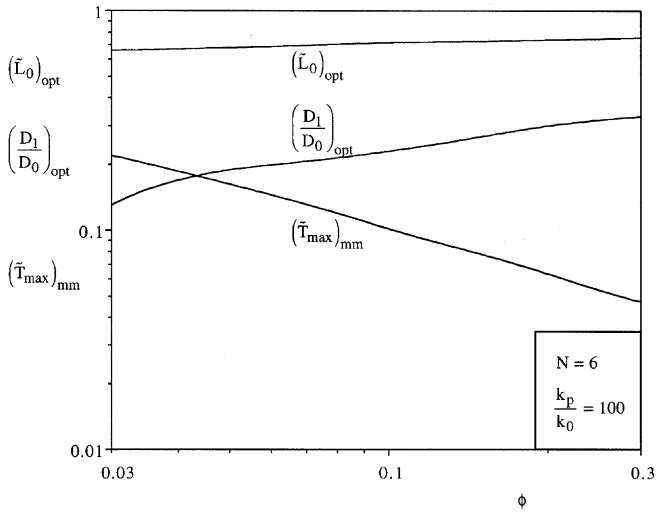

Fig. 4. The effect of the high-conductivity volume fraction ϕ on the optimized structure of Fig. 1.

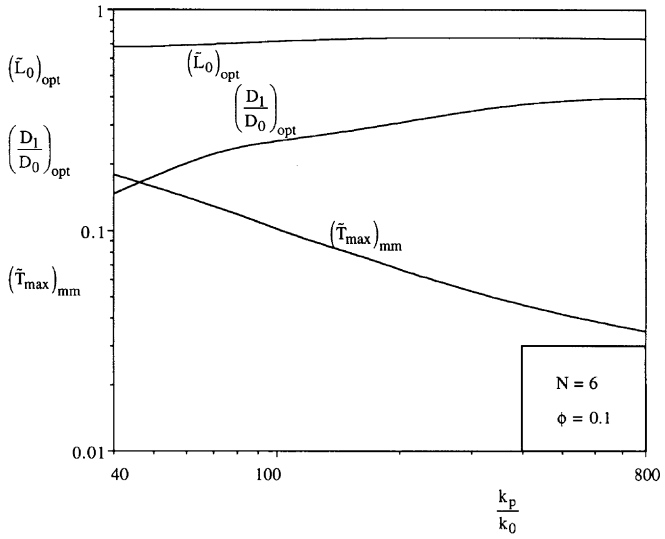

Fig. 5. The effect of the ratio of conductivities k_p/k_0 on the optimized structure of Fig. 1.

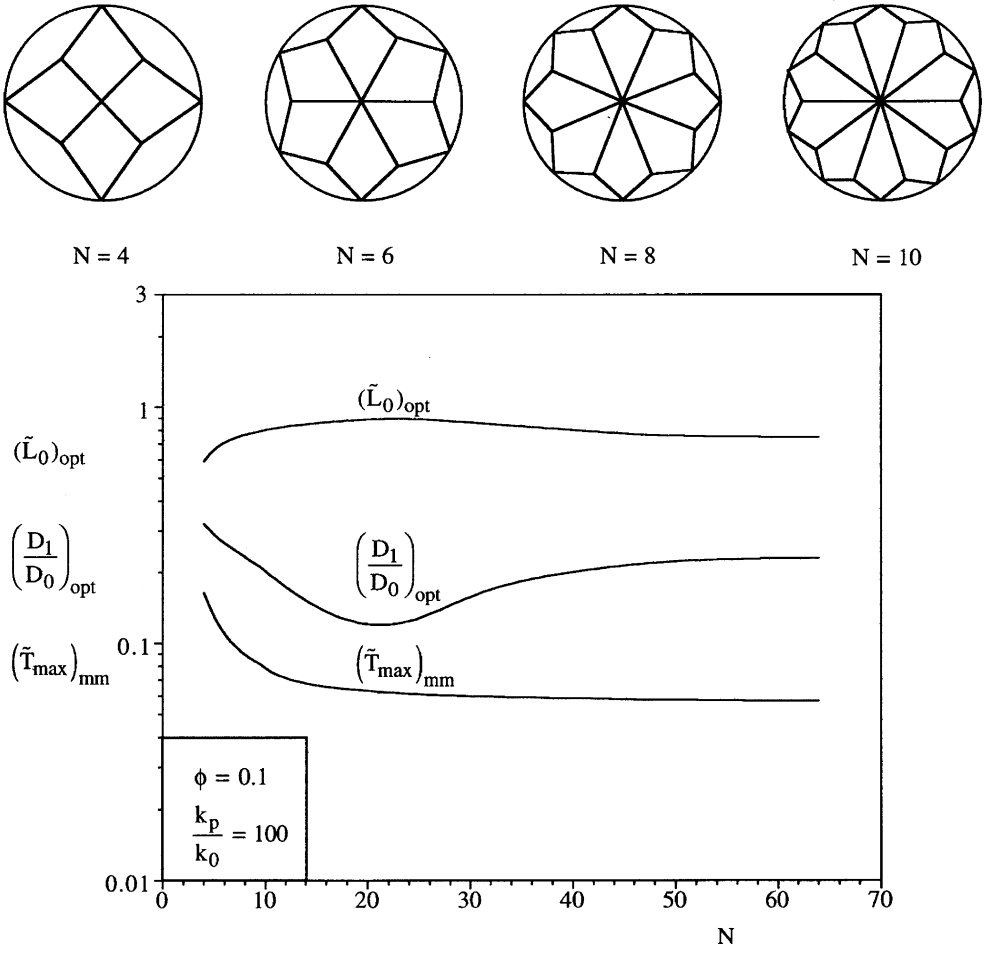

Fig. 6. The effect of the size of the disc on the optimized structure of Fig. 1.

realistic in the present geometry. Note further that the numerical and analytical results shown in Table 2 are non-dimensionalized in accordance with Ref. [27], namely, $\widetilde{R} = R_0/A_1^{1/2}$ and $\widetilde{T}_{max} = (T_{max} - T_{min})/(q'''A_1^{1/2}/k_0)$, where the elemental area A_1 is shown in the upper part of Fig. 8.

Fig. 2 shows the first stage of geometric optimization. The global resistance has a minimum with respect to the bifurcation radius $\widetilde{L}_0$, when the other degree of freedom (D_1/D_0) and constraints (N, k_p/k_0, ϕ) are specified. The lower part of Fig. 2 shows how $\widetilde{L}_1$ and β vary as $\widetilde{L}_0$ changes.

The optimization illustrated in Fig. 2 was performed for many values of D_1/D_0, and the optimization results are summarized in Fig. 3. There are two results, the optimized radial blade length $\widetilde{L}_0$, which is practically independent of D_1/D_0, and the minimized global resistance $(\widetilde{T}_{max})_{min}$, which has a shallow minimum with respect to D_1/D_0. We denote this smallest of all $(\widetilde{T}_{max})_{min}$ values by $(\widetilde{T}_{max})_{mm}$. The configuration that corresponds to $(\widetilde{T}_{max})_{mm}$ has been drawn to scale in the inset of Fig. 3.

To summarize, the conductive flow structure can be optimized with respect to two free geometric features, $\widetilde{L}_0$ and D_1/D_0. In Figs. 4–6 we explored the sensitivity of the optimized configuration to changes in the constraints. Figs. 4 and 5 show that the radius of bifurcation $(\widetilde{L}_0)_{opt}$ is relatively insensitive to changes in both ϕ and k_p/k_0. We may

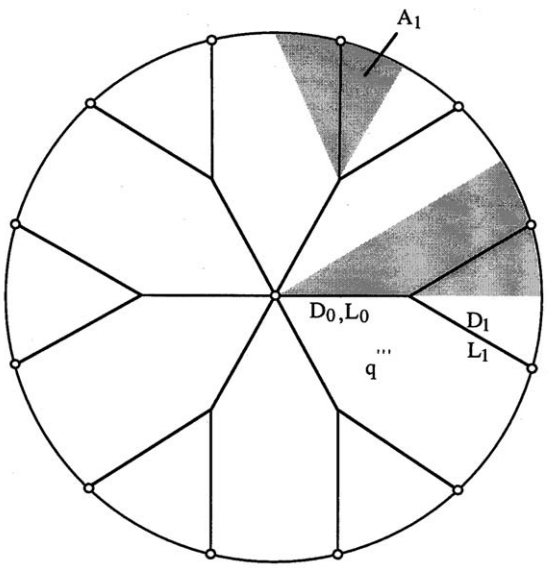

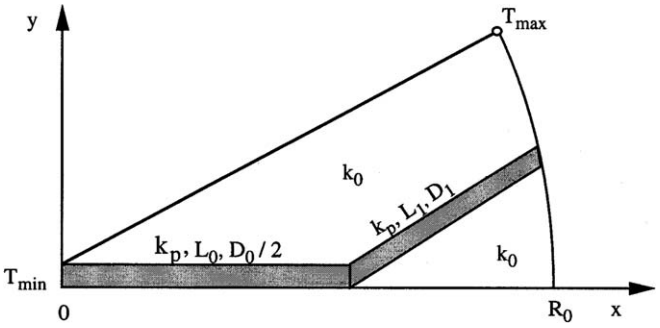

Fig. 8. Design with one level of bifurcation.

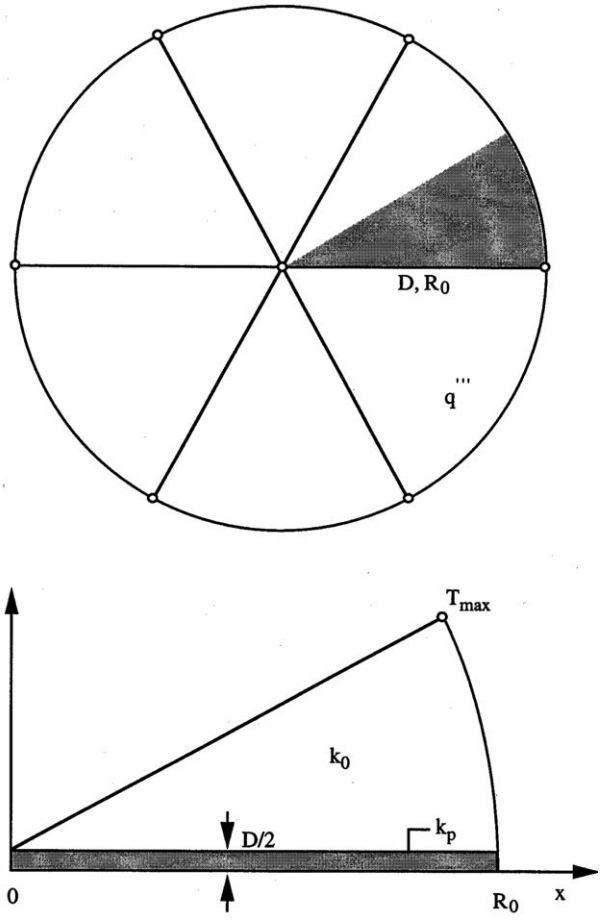

Fig. 7. Design with radial blades.

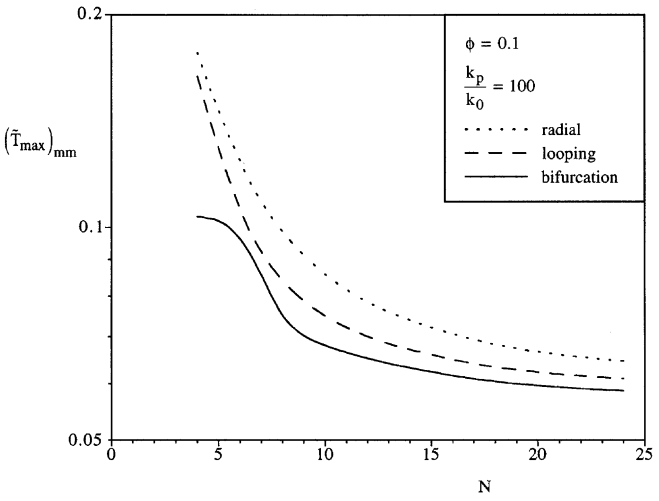

Fig. 9. The minimized overall thermal resistance as function of the number of central blades.

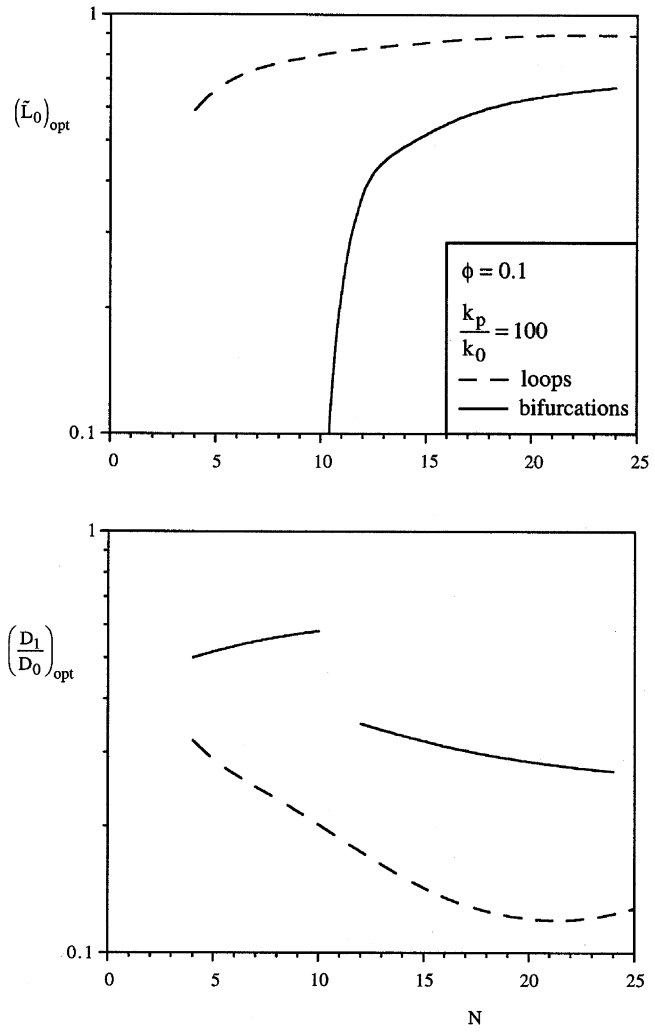

Fig. 10. The effect of the number of central blades N on the optimal central blade length $(\widetilde{L}_0)_{opt}$ and optimal ratio $(D_1/D_0)_{opt}$.

take $\widetilde{L}_0 \cong 0.7$ as a representative value for all the optimized configurations that have $N = 6$ points on the rim. Figs. 4 and 5 also show that the ratio of blade thicknesses $(D_1/D_0)_{opt}$ increases weakly as either ϕ or k_p/k_0 increase. This trend is reasonable because in this direction the peripheral branches become more effective as conduits for heat flow, hence their increasing thickness. In the same direction, the minimized global thermal resistance decreases. In the ϕ and k_p/k_0 ranges covered by Figs. 4 and 5, the minimized global conductance varies roughly as

$$(T_{max})_{mm} = 0.27\phi^{-0.67}(k_p/k_0)^{-0.56} \tag{8}$$

In Fig. 6 we show how the optimized structure and its global performance respond to changes in global size (R_0), when the spacing between k_p points on the rim (d) is fixed. This is equivalent to changing the number of k_p points on the rim, or the number of radial blades N. The disc radius increases in proportion with N, namely $R_0 = Nd/(2\pi)$. One important conclusion is that the dimensionless minimized global thermal resistance decreases significantly with the size of the system until N is approximately equal to 20, beyond which $(\widetilde{T}_{max})_{min}$ is less sensitive to changes in the value of N.

3. Comparison between radial, one-bifurcation and one-loop designs

The radial design is shown in Fig. 7. The structure consists of N blades of high-conductivity (k_p) embedded in a heat generating disc of radius R_0 and lower conductivity k_0. The blades have the length R_0 and thickness D. The global thermal resistance of this flow structure is expressed in dimensionless form by Eq. (1). The area of the sector shown in Fig. 7 is given by Eq. (2). The area occupied by the k_p material is now given by

$$A_p = R_0 D \tag{9}$$

The fixed volume fraction occupied by the k_p material is given by Eq. (4). The model consists of Eqs. (5) and (6) and the boundary conditions presented in Section 2.

The design with one level bifurcation is shown in Fig. 8: one k_p blade stretches radially to the distance L_0 from the central heat sink, and continues with two tributary branches that reach the rim. Each tributary branch reaches the rim in the middle of the sector shown in Fig. 8. The analysis used for the design with one loop size continues to hold, Eqs. (1)–(7).

We solved Eqs. (5) and (6) subjected to the constraints (2) and (4). The boundary conditions are the same as in Section 2: the perimeter of the sector of area A_0 is insulated, with the exception of the heat sink T_{mim}. Fig. 9 shows that the global thermal resistance decreases when the number of the radial blades increases. The design with one level of bifurcation performs better than the design with one loop in size. Both designs perform better than the radial design when they are compared based on the same number of central blades N. However, if they are compared with the radial structure with $2N$ central blades, the radial design performs better than the bifurcated design when $N \leqslant 10$. Said another way, in the bifurcated design $L_{0,opt}$ vanishes when $N \leqslant 10$ (Fig. 10), and the optimal bifurcated structure becomes a radial structure with $2N$ blades. This is why in Fig. 9 the curve for bifurcated structures merges with the curve for radial structures with $2N$ blades at $N \sim 10$.

Fig. 10 shows that the optimal length of the central blade $(\widetilde{L}_0)_{opt}$ in the design with one level of bifurcation is smaller than $(\widetilde{L}_0)_{opt}$ of the design with one loop size. In the design with one level of bifurcation the length $(\widetilde{L}_0)_{opt}$ tends to zero. This means that when $N \leqslant 10$ the best design with one level of bifurcation is a radial design with $2N$ central blades.

The lower part of Fig. 10 shows the effect of N on the ratio $(D_1/D_0)_{opt}$ in the design with one level of bifurcation and one loop size. The $(D_1/D_0)_{opt}$ ratio of the design with

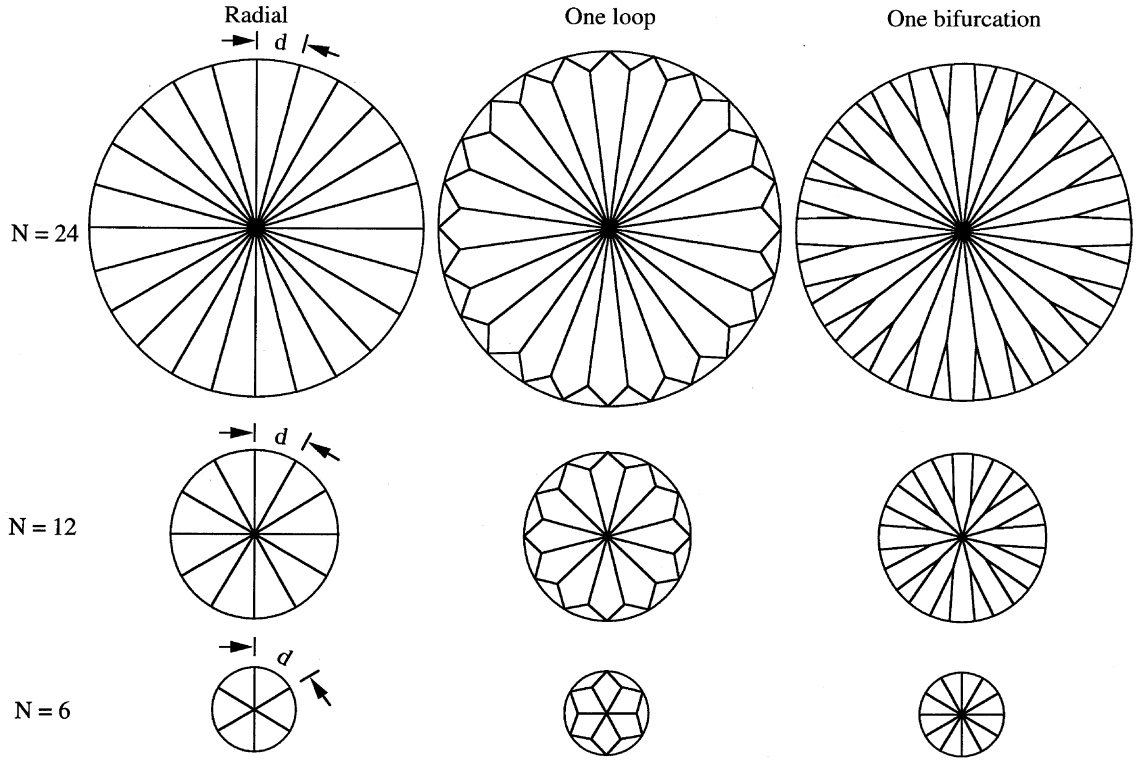

Fig. 11. Optimized structures with the same smallest scale (d) and increasing size (N or R).

loops is smaller. See again the discontinuity at $N \cong 10$, which is due to the disappearance of $L_{0,\mathrm{opt}}$ when $N \leqslant 10$. Fig. 11 shows examples of the optimized structures documented in Figs. 9 and 10. The smallest length scale (d) is the same in every design, while N (or R) varies. When N (or R) is fixed the global performance increases from left to right.

4. Two loop sizes, two branching levels

Considerably more complicated than the configuration optimized until now is the configuration of Fig. 12, where there are two characteristic loops, both quadrilateral. One loop has two radial blades L_0 and two branches L_1, while the other has two branches L_1 and two branches L_2. The respective thicknesses of the blades are D_0, D_1 and D_2. The number of k_p points on the rim (N) is the same as the number of radial blades. The disc radius is R_0, and, according to the first of Eq. (7), the dimensionless lengths of the design are $(\widetilde{L}_i, \widetilde{D}_i) = (L_i, D_i)/R_0$. The relative amount of high-conductivity material, ϕ, is defined in a way that is consistent with Eqs. (2)–(4), namely

$$\phi = \frac{N}{\pi R_0^2}\left(D_0 L_0 + 2D_1 L_1 + 2D_2 L_2\right) \tag{10}$$

When ϕ, N and k_p/k_0 are fixed, the design has four degrees of freedom, two length ratios, and two thickness ratios, for example, $\widetilde{L}_0$, $\widetilde{L}_2$, D_1/D_0 and D_2/D_0. We simulated steady conduction with uniform heat generation in a very large number of configurations, and we identified the changes in geometry that cause decreases in the hot spot temperature $\widetilde{T}_{\max}$, regardless of its location. We conducted this search hierarchically, in four nested levels.

At the innermost level, we fixed $\widetilde{L}_0$, D_1/D_0 and D_2/D_0, and varied $\widetilde{L}_2$ until $\widetilde{T}_{\max}$ reached its lowest value. An example of a search at this level is shown in Fig. 12. Noteworthy is the shallowness of the minimum exhibited by $\widetilde{T}_{\max}$. This means that the accurate selection of the most peripheral length $\widetilde{L}_2$ is not a critical design decision. This quality (robustness) of complex flow structures was encountered before, for example in the performance of conduction trees with two or more levels of pairing or bifurcation [2]. It was found that complex flow structures in which not every feature is optimized perform at nearly the same level as fully-optimized structures.

At the next level, the optimum identified at the first level $[(\widetilde{T}_{\max})_{\min}]$ was generated for a new class of configurations in which D_2/D_0 varied (in addition to $\widetilde{L}_2$), while $\widetilde{L}_0$ and D_1/D_0 remained fixed. In this way, we found how $(\widetilde{T}_{\max})_{\min}$ varies with D_1/D_0, and were able to determine the design with the smallest of all the $(\widetilde{T}_{\max})_{\min}$ values, which is labeled $(\widetilde{T}_{\max})_{\mathrm{mm}}$. The optimal ratio D_2/D_0 determined in Fig. 13 is labeled $(D_2/D_0)_\mathrm{o}$.

The procedure used in Figs. 12 and 13 was repeated by keeping $\widetilde{L}_0$ constant and varying the ratio D_1/D_0. The results are summarized in Fig. 14, which shows that there is an optimal ratio of blade thicknesses, $(D_1/D_0)_\mathrm{o}$. The corresponding values at this optimum are the minimized

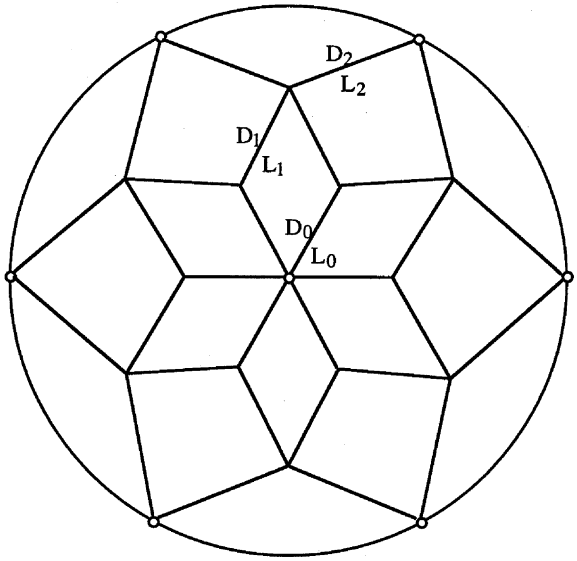

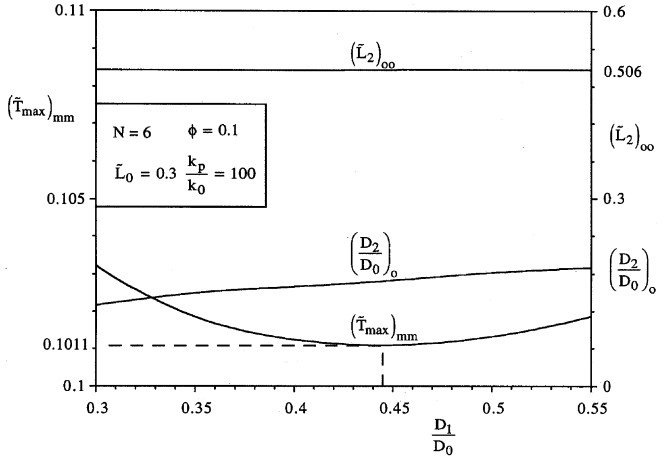

Fig. 14. The minimization with respect to D_1/D_0 of the global thermal resistance already minimized with respect to $\widetilde{L}_2$ and D_2/D_0.

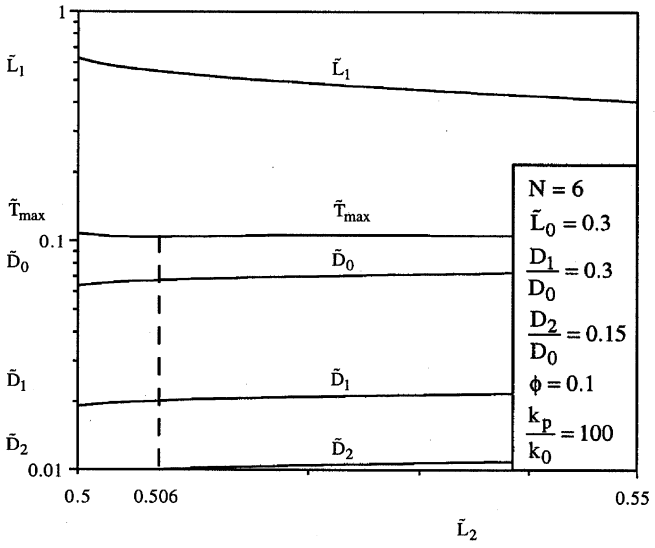

Fig. 12. Design with loops of two sizes and two levels of bifurcation, and optimization by varying the peripheral length $\widetilde{L}_2$.

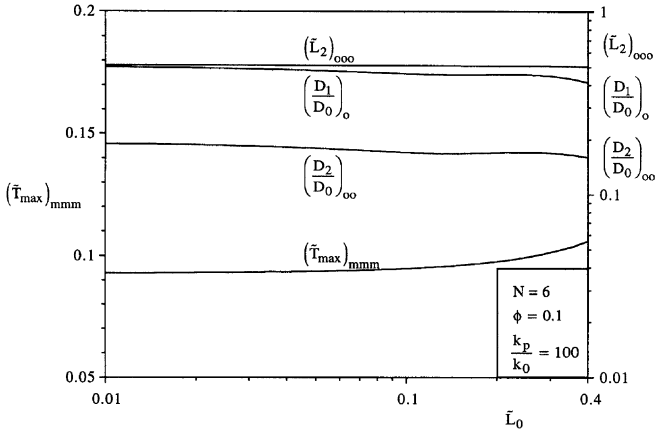

Fig. 15. The effect of the central blade length $\widetilde{L}_0$ on the global thermal resistance already minimized with respect to $\widetilde{L}_2$, D_2/D_0, and D_1/D_0.

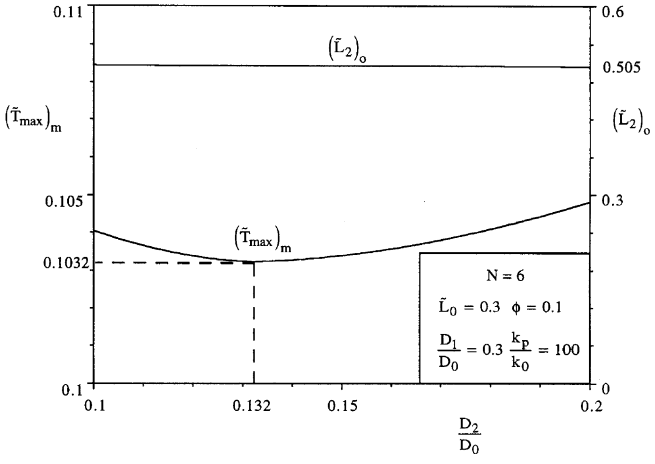

Fig. 13. The minimization with respect to D_2/D_0 of the global thermal resistance already minimized with respect to the peripheral length $\widetilde{L}_2$.

global resistance $(\widetilde{T}_{\max})_{\mathrm{mmm}}$, the optimal ratio $(D_2/D_0)_{\mathrm{oo}}$, and the optimal length $(\widetilde{L}_2)_{\mathrm{ooo}}$.

In the final optimization stage (the outermost loop), we exploited the fourth degree of freedom, $\widetilde{L}_0$. Fig. 15 shows that $(\widetilde{T}_{\max})_{\mathrm{mmm}}$ decreases monotonically as $\widetilde{L}_0$ vanishes. In this limit, the optimal two-loop structure becomes the same as the optimal one-loop structure studied in Section 2. Fig. 16 shows four examples of the structures optimized in Fig. 15.

We repeated the procedure of Figs. 12–15 by assuming N values other than 6 for the number of central blades, namely $N = 9$, 12, 24, 32, 48 and 64. Fig. 17 is another example ($N = 9$) of the structures optimized according to the procedure used in Figs. 12–15. The results show that the optimized one-loop design always performs better than the optimized two-loop design. In other words, the message of Fig. 15 is general: the optimal L_0 is zero, and the optimized two-loop size structure becomes an optimized one-loop size structure.

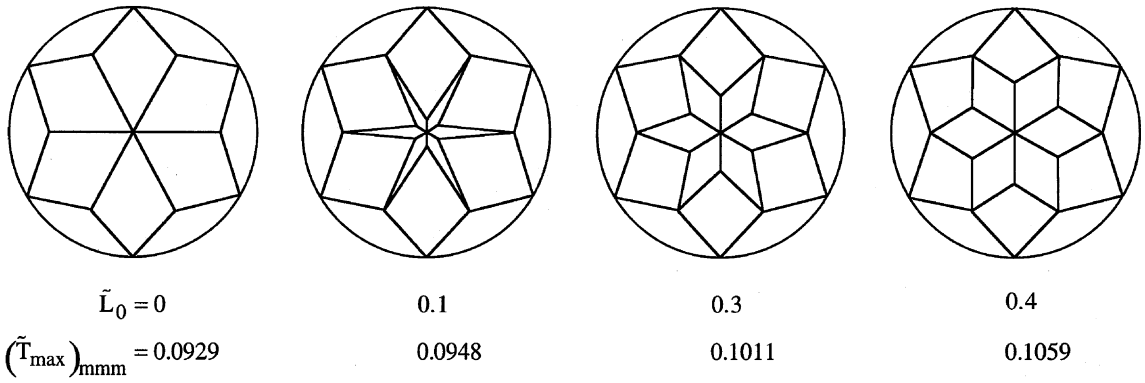

Fig. 16. Examples of the optimized structures documented in Fig. 15 ($N = 6$).

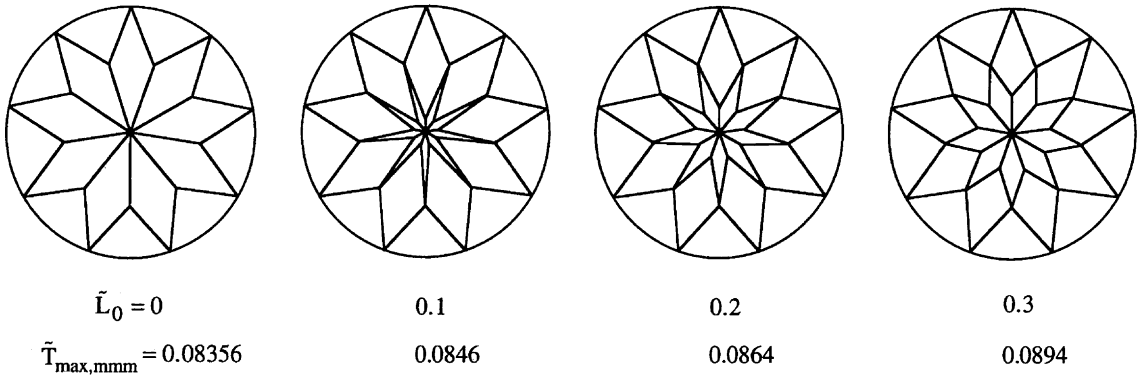

Fig. 17. Examples of optimized structures with $N = 9$.

5. Concluding remarks

In this study we looked in detail at how the generation of tree architectures with loops enhances the performance of conduction cooling of bodies that generate heat volumetrically. The main conclusion is summarized graphically by Fig. 11. When the smallest length scale of the design (d) is constrained, performance improves as the structure evolves from radial to 'with loops' and, finally, dendritic. Well defined boundaries (transitions) separate these classes of architectures in the performance domain.

In the second part of this study we found that if we complicate the design by using two loop sizes (Fig. 12), the optimized structure evolves toward one with loops of only one size (Fig. 15). This evolution, however, is very gentle in that the global performance and optimized geometric features do not change much from one configuration to the next. There are many configurations with two loop sizes that perform nearly as well as the best configuration. This finding is another illustration of how complex flow structures exhibit robustness, such that in the vicinity of the *equilibrium flow structure* [4,5] reside many configurations that have nearly the same global performance level.

By comparing Fig. 12 with Fig. 3 we see that conduction trees with two loop sizes are marginally inferior to trees with only one loop size: then why should designers be interested in tree structures with multi-scale loops? Robustness is one reason, because more scales mean more degrees of freedom en route to the optimized multi-loop structure. Robustness also means that the global performance of the cooling structure does not change much if the structure is damaged locally. Another advantage of the structure with more loop sizes is that, locally, it spreads the temperature more uniformly even though its peak temperature is slightly higher than in the corresponding structure with only one loop size.

Constructal theory and design is now a growing field: Refs. [3–5,29–33] illustrate the more recent work and new directions.

Acknowledgement

Prof. Luiz Rocha's work was sponsored by FAPERGS, Porto Alegre, RS, Brazil.

References

[1] A. Bejan, Advanced Engineering Thermodynamics, second ed., Wiley, New York, 1997 (Chapter 13).
[2] A. Bejan, Shape and Structure, from Engineering to Nature, Cambridge University Press, Cambridge, UK, 2000.
[3] A. Bejan, I. Dincer, S. Lorente, A.F. Miguel, A.H. Reis, Porous and Complex Flow Structures in Modern Technologies, Springer-Verlag, New York, 2004.
[4] A. Bejan, S. Lorente, La Loi Constructale, L'Harmattan, Paris, 2005.

[5] A. Bejan, S. Lorente, The constructal law and the thermodynamics of flow systems with configuration, Int. J. Heat Mass Transfer 47 (2004) 3203–3214.
[6] D. Tondeur, L. Luo, U. D'Ortona, Optimisation des transferts et des matériaux par l'approche constructale, Entropie 224/225 (2000) 32–37.
[7] G. Hernandez, Design of platforms for customizable products as a problem of access in a geometric space, PhD thesis, Georgia Institute of Technology, Atlanta, GA, 2001.
[8] Y. Chen, P. Cheng, Heat transfer and pressure drop in fractal tree-like microchannel nets, Int. J. Heat Mass Transfer 45 (2002) 2643–2648.
[9] D.V. Pence, Reduced pumping power and wall temperature in microchannel heat sinks with fractal-like branching channel networks, Microscale Thermophys. Eng. 6 (2002) 319–330.
[10] Z.-Z. Xia, Z.-X. Li, Z.-Y. Guo, Heat conduction optimization: high conductivity constructs based on the principle of biological evolution, in: 12th Int. Heat Transfer Conf., Grenoble, France, 18–23 August 2002.
[11] G. Hernandez, J.K. Allen, F. Mistree, Design of hierarchic platforms for customizable products, ASME Paper DETC2002/DAC-34095, Proceedings of DETC'02, ASME 2002 Design Engineering Technical Conferences and Computer and Information in Engineering Conference, Montreal, Canada, September 29–October 2, 2002.
[12] M.J. Carone, C.B. Williams, J.K. Allen, F. Mistree, An application of constructal theory in the multi-objective design of product platforms, ASME Paper DETC2003/DTM-48667, Proceedings of DETC'03, ASME 2003 Design Engineering Technical Conferences and Computers and Information in Engineering Conference, Chicago, Illinois, September 2–6, 2003.
[13] H. Brod, Residence time optimized choice of tube diameters and slit heights in distribution systems for non-Newtonian liquids, J. Non-Newton. Fluid Mech. 111 (2003) 107–125.
[14] G. Hernandez, J.K. Allen, F. Mistree, Platform design for customizable products as a problem of access in a geometric space, Eng. Optim. 35 (2003) 229–254.
[15] J. Lewins, Bejan's constructal theory of equal potential distribution, Int. J. Heat Mass Transfer 46 (2003) 1541–1543.
[16] L. Ghodoossi, N. Egrican, Exact solution for cooling of electronics using constructal theory, J. Appl. Phys. 93 (8) (2003) 4922–4929.
[17] B. A/K Abu-Hijleh, Optimized use of baffles for reduced natural convection heat transfer from a horizontal cylinder, Int. J. Therm. Sci. 42 (2003) 1061–1071.
[18] L. Luo, D. Tondeur, A. Gruss, Intensification des transferts et conception des échangeurs multi-échelles, Congrés Français de Thermique, SFT 2003, Grenoble, 3–6 June 2003.
[19] M.J. Carone, Applying constructal theory for product platform design in the context of group decision-making and uncertainty, MS thesis, Georgia Institute of Technology, Atlanta, GA, 2003.
[20] W. Nakayama, A methodology to work on geometrically complex heat transfer systems: the cases of heat conduction through composite slabs, Int. J. Heat Mass Transfer 46 (2003) 3397–3409.
[21] Y. Azoumah, N. Mazet, P. Neveu, Constructal network for heat and mass transfer in a solid–gas reactive porous medium, Int. J. Heat Mass Transfer 47 (2004) 2961–2970.
[22] S.M. Senn, D. Poulikakos, Laminar mixing, heat transfer and pressure drop in tree-like microchannel nets and their application for thermal management in polymer electrolyte fuel cells, J. Power Sources 130 (2004) 178–191.
[23] S.M. Senn, D. Poulikakos, Tree network channels as fluid distributors constructing double-staircase polymer electrolyte fuel cells, J. Appl. Phys. 96 (1) (2004) 842–852.
[24] M.A. Almogbel, Constructal tree-shaped fins, Int. J. Therm. Sci. 44 (2005) 342–348.
[25] A.K. Pramanick, P.K. Das, Note on constructal theory of organization in nature, Int. J. Heat Mass Transfer 48 (2005) 1974–1981.
[26] L. Gosselin, Minimum pumping power fluid tree networks without a priori flow regime assumption, Int. J. Heat Mass Transfer 48 (2005) 2159–2171.
[27] L.A.O. Rocha, S. Lorente, A. Bejan, Constructal design for cooling a disc-shaped area by conduction, Int. J. Heat Mass Transfer 45 (2002) 1643–1652.
[28] MATLAB, User's Guide, Version 6.0.088, release 12, The Mathworks, Inc., 2000.
[29] H. Poirier, Une théorie explique l'intelligence de la nature, Sci. Vie 1034 (November) (2003) 44–63.
[30] R.N. Rosa, A.H. Reis, A.F. Miguel, Bejan's Constructal Theory of Shape and Structure, Évora Geophysics Center, University of Évora, Portugal, 2004.
[31] A.K. Pramanick, P.K. Das, Constructal design of a thermoelectric device, Int. J. Heat Mass Transfer 49 (2006) 1420–1429.
[32] A. Bejan, Advanced Engineering Thermodynamics, third ed., Wiley, Hoboken, NJ, 2006.
[33] A.H. Reis, Constructal theory: from engineering to physics, and how flow systems develop shape and structure, Appl. Mech. Rev. 59 (2006), in press.